Article

Developmental Cell

Foxf2 Is Required for Brain Pericyte Differentiation and Development and Maintenance of the Blood-Brain Barrier

Highlights

- The transcription factor Foxf2 is expressed specifically in CNS pericytes
- *Foxf2*$^{-/-}$ mice have cerebrovascular defects and fail to develop a blood-brain barrier
- *Foxf2*$^{-/-}$ CNS vasculature has reduced Pdgfrβ and Tgfβ-Smad2/3 signaling
- Inactivation of *Foxf2* in adult mice leads to breakdown of the blood-brain barrier

Authors

Azadeh Reyahi, Ali M. Nik, Mozhgan Ghiami, ..., Fredrik Pontén, Bengt R. Johansson, Peter Carlsson

Correspondence

peter.carlsson@cmb.gu.se

In Brief

Pericytes induce formation of the blood-brain barrier (BBB), but it is not clear why only pericytes in the CNS have this unique capability. Reyahi et al. identify the forkhead transcription factor Foxf2 as being expressed specifically in CNS pericytes and as being required for BBB formation and maintenance.

Reyahi et al., 2015, Developmental Cell *34*, 19–32
July 6, 2015 ©2015 Elsevier Inc.
http://dx.doi.org/10.1016/j.devcel.2015.05.008

CellPress

Developmental Cell
Article

Foxf2 Is Required for Brain Pericyte Differentiation and Development and Maintenance of the Blood-Brain Barrier

Azadeh Reyahi,[1] Ali M. Nik,[1] Mozhgan Ghiami,[1] Amel Gritli-Linde,[2] Fredrik Pontén,[3] Bengt R. Johansson,[4] and Peter Carlsson[1,*]
[1]Department of Chemistry and Molecular Biology, University of Gothenburg, Box 462, 405 30 Gothenburg, Sweden
[2]Department of Oral Biochemistry, Sahlgrenska Academy, University of Gothenburg, Box 450, 405 30 Gothenburg, Sweden
[3]Department of Immunology, Genetics and Pathology, Rudbecklaboratoriet, Uppsala University, 751 85 Uppsala, Sweden
[4]Institute of Biomedicine, University of Gothenburg, Box 440, 405 30 Gothenburg, Sweden
*Correspondence: peter.carlsson@cmb.gu.se
http://dx.doi.org/10.1016/j.devcel.2015.05.008

SUMMARY

Pericytes are critical for cerebrovascular maturation and development of the blood-brain barrier (BBB), but their role in maintenance of the adult BBB, and how CNS pericytes differ from those of other tissues, is less well understood. We show that the forkhead transcription factor Foxf2 is specifically expressed in pericytes of the brain and that *Foxf2*$^{-/-}$ embryos develop intracranial hemorrhage, perivascular edema, thinning of the vascular basal lamina, an increase of luminal endothelial caveolae, and a leaky BBB. *Foxf2*$^{-/-}$ brain pericytes were more numerous, proliferated faster, and expressed significantly less Pdgfrβ. Tgfβ-Smad2/3 signaling was attenuated, whereas phosphorylation of Smad1/5 and p38 were enhanced. Tgfβ pathway components, including Tgfβ2, Tgfβr2, Alk5, and integrins $\alpha_V\beta_8$, were reduced. *Foxf2* inactivation in adults resulted in BBB breakdown, endothelial thickening, and increased trans-endothelial vesicular transport. On the basis of these results, *FOXF2* emerges as an interesting candidate locus for stroke susceptibility in humans.

INTRODUCTION

The demands on the vasculature vary widely among organs, and the endothelium differs accordingly in characteristics such as permeability to water, metabolites, macromolecules, and cells. Genetic and co-culture experiments indicate that, rather than being intrinsically different, endothelial cells adopt the phenotype specific to each tissue in response to their environment. This is particularly well illustrated by the vasculature of the CNS, where passive passage between the blood and the brain parenchyma has been brought to a minimum. The intimately connected cells of the neurovascular unit—astrocytes, microglia, neurons, and mural cells (i.e., pericytes in capillaries and vascular smooth muscle cells [vSMCs] in arteries)—tightly control metabolite exchange, blood flow, and endothelial permeability. This blood-brain barrier (BBB) minimizes intercellular passage with tight junctions between endothelial cells and non-specific trans-endothelial exchange by reduced vesicular transport. Endothelial shuttling of metabolites is instead handled by a range of selective transporters (Zlokovic, 2008).

Restriction of cerebrovascular permeability already occurs during embryonic development, in mice about a week before astrocyte differentiation and coincident with pericyte colonization (Daneman et al., 2010). Loss of platelet-derived growth factor B (Pdgfb) in endothelium, or its receptor Pdgf receptor β (Pdgfrβ) in mural cells, inhibits proliferation and migration of pericytes and results in severe pericyte deficiency in many organs, including the CNS (Levéen et al., 1994; Lindahl et al., 1997; Soriano, 1994). The phenotypes of hypomorphic alleles and gene dosage alterations support a dose-response relationship between Pdgfb signaling and pericyte investment in the CNS and show that vascular permeability correlates inversely with the degree of pericyte coverage (Armulik et al., 2010; Daneman et al., 2010).

In avian embryos, pericytes and vSMCs of the forebrain are derived from cephalic neural crest, whereas those posterior of the mesencephalon-prosencephalon boundary are mesodermal (Etchevers et al., 2001; Korn et al., 2002; Kurz, 2009). The origin of mammalian mural cells has not been as rigorously traced, but marker analysis suggests that neural crest contributes most, if not all, perivascular cells also in the posterior parts of the brain (Armulik et al., 2011; Heglind et al., 2005). To what extent induction of BBB relies on unique properties of CNS pericytes is not well understood, but lineage does not appear to be critical, because mural cells of thymus and some craniofacial tissues are derived from neural crest (Etchevers et al., 2001; Foster et al., 2008), and avian CNS pericytes are of mixed origin.

In addition to Pdgfb/Pdgfrβ, several paracrine and juxtacrine pathways have been implicated in pericyte-endothelial signaling (for a review, see Armulik et al., 2011). Tgfβ is particularly pleiotropic and controls proliferation, migration, and differentiation of both pericytes and endothelial cells (reviewed by Gaengel et al., 2009; Winkler et al., 2011). Activation of latent Tgfβ requires intimate contact between the two cell types (Sato and Rifkin, 1989), involving the gap junction protein connexin 43 (Hirschi et al., 2003), and physical interaction with integrins $\alpha_V\beta_8$ (Bader et al.,

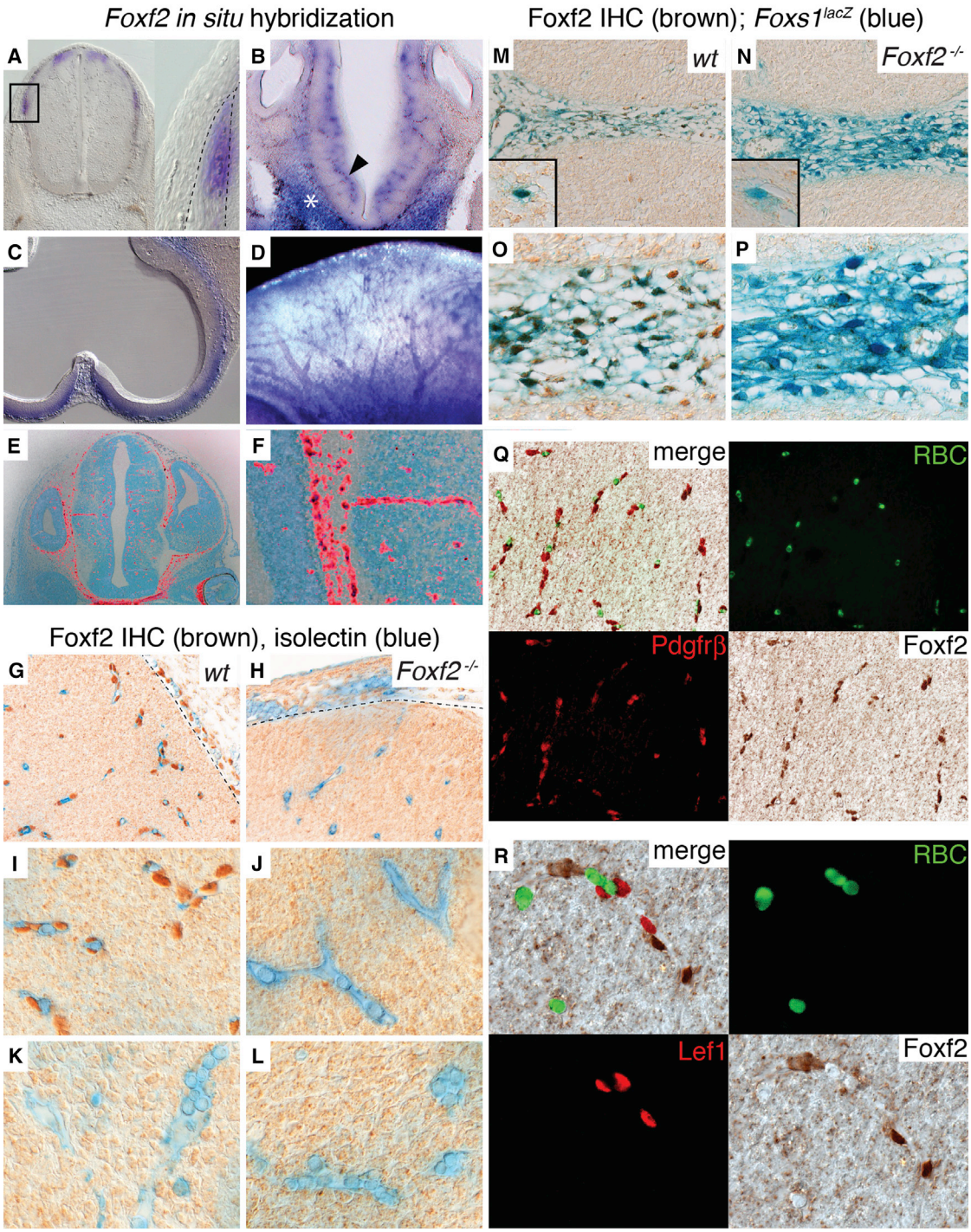

Figure 1. Expression of *Foxf2* in Neural Crest-Derived Pericytes in the Brain

(A–D) *Foxf2* whole-mount in situ hybridization of mouse embryos. (A) *Foxf2* expression in nascent neural crest. Dashed line indicates boundaries between surface ectoderm, neural crest mesenchyme, and neuroectoderm. (B) *Foxf2*+ cells in head mesenchyme (asterisk) and associated with sprouting blood vessels (arrowhead) in E10.5 hindbrain. (C) *Foxf2*+ cells in perineural mesenchyme surrounding E10.5 forebrain. (D) Profile of whole E11.5 head with *Foxf2* expression associated with the cranial vasculature.

(E) *Foxf2* radioactive in situ hybridization (red) of E14.5 forebrain section with *Foxf2*+ expression in perineural mesenchyme and associated with the cerebral vasculature.

(F) Detail from (E).

(legend continued on next page)

1998; Cambier et al., 2005; Shi et al., 2011; Wipff and Hinz, 2008; Zhu et al., 2002). The net effect of Tgfβ signaling is determined by the relative activities of two competing and antagonistic pathways, each mediated by a distinct type 1 receptor (Goumans et al., 2002, 2003). Alk5-Smad2/3 increases production of extracellular matrix of the vascular basal lamina, inhibits proliferation and migration, and promotes differentiation of both endothelial cells and pericytes. Alk1-Smad1/5 signaling has essentially the opposite effect.

We describe the consequences for the brain vasculature of targeting *Foxf2*, encoding a forkhead transcription factor. *Foxf2*, and the closely related *Foxf1*, are expressed in tissues derived from the splanchnic and head mesoderm, and have partially overlapping roles in the development of endodermal organs and the secondary palate (Astorga and Carlsson, 2007; Mahlapuu et al., 2001a, 2001b; Wang et al., 2003). *Foxf2* controls gut development (Ormestad et al., 2006), a function conserved between mammals and *Drosophila* (Jakobsen et al., 2007), and is a mesenchymal regulator of the intestinal stem cell niche (Nik et al., 2013). *Foxf2* is also expressed in neural crest (Ormestad et al., 2004), but the significance of this for embryonic development has remained elusive. Here, we show that *Foxf2*-expressing neural crest cells are progenitors of cerebrovascular mural cells and that inactivation of *Foxf2* leads to hyperplasia and defective differentiation of brain pericytes, a leaky BBB, and attenuation of Pdgfrβ and Tgfβ-Smad2/3 signaling.

RESULTS

Foxf2 Is Expressed in Neural Crest-Derived Cerebrovascular Pericytes

During murine embryonic development, *Foxf2* expression is activated in neural crest (Figure 1A) around E9.5 (Ormestad et al., 2004). At E10.5, *Foxf2* mRNA is found in head mesenchyme and is associated with the hindbrain vasculature (Figure 1B). *Foxf2* expression is also seen in the perineural mesenchyme around the mid- and forebrain (Figure 1C) and is from E11.5 associated with blood vessels throughout the brain (Figures 1D–1F). This pattern is characteristic of neural crest-derived progenitors of CNS mural cells, which migrate anteriorly/ventrally in the perineural mesenchyme and enter the neuroectoderm along the paths of the angiogenic sprouts that penetrate the developing brain from the surrounding vascular plexus (Daneman et al., 2010; Heglind et al., 2005; Yamanishi et al., 2012). No *Foxf2* expression was seen associated with blood vessels outside the brain (Figures 1B and 1E).

To confirm the identity of *Foxf2*-expressing cells, we immunolocalized Foxf2 in the developing brain. The anti-Foxf2 antibody has a strong cross-reactivity with a pan-neuronal epitope (Nik et al., 2013), which makes it inappropriate for use in the mature brain, but until E12.5, the non-specific cytoplasmic staining remains manageable. Foxf2+ nuclei were associated with blood vessels (identified by isolectin staining) inside the brain (Figures 1G and 1I) but not in head mesenchyme (Figure 1K) and were absent from *Foxf2*$^{-/-}$ embryos (Figures 1H, 1J, and 1L). In embryos with a *lacZ* knockin allele of *Foxs1*, a neural crest marker that in mid- and forebrain is expressed only in vascular mural cells (Heglind et al., 2005), Foxf2 co-localized with the β-gal+ nuclei of *Foxs1*^{lacZ}-expressing cells, both in the perineural mesenchyme (Figures 1M and 1O) and in the brain (Figure 1M, inset). The specificity was verified by the absence of nuclear staining in sections from *Foxf2*$^{-/-}$ embryos (Figures 1N and 1P). Cells with Foxf2+ nuclei expressed Pdgfrβ (Figure 1Q) but were negative for Lef1 (Figure 1R), a nuclear protein present in all endothelial cells in the brain (Siegenthaler et al., 2013). Together, these results are consistent with *Foxf2*-expressing cells in the embryonic brain being pericytes and precursors of vSMCs.

Apart from the CNS, neural crest-derived pericytes also occur in thymus (Foster et al., 2008). To investigate if *Foxf2* expression reflects lineage or is specific for CNS pericytes, we first confirmed that the thymic vasculature contains cells of neural crest origin by using mice transgenic for the *mTmG* dual fluorescent marker (Muzumdar et al., 2007) and *Wnt1-Cre* (Danielian et al., 1998), which gives neural crest-derived cells membrane-localized enhanced GFP (EGFP) (green), whereas other cells have tdTomato (red) fluorescence (Figure S1A available online). Whereas Foxf2+ nuclei were detected in fibroblasts of intestinal villi (Figure S1C) and along capillaries throughout the CNS, including in the spinal cord (Figure S1D), no cells in the thymus expressed Foxf2 (Figure S1B). Foxf2 is therefore a good candidate for a factor that distinguishes brain pericytes from those of extra-neuronal tissues, independent of lineage.

Abnormal Cerebral Capillaries in *Foxf2*$^{-/-}$ Embryos

The gross morphology of the CNS vasculature was examined in E18.5 *mTmG;Tie2-Cre*, in which endothelial cells express EGFP. No difference in angiogenesis (capillary density, branching frequency) was detected between wild-type and *Foxf2*$^{-/-}$ brains (Figure S2A). In cross section, however, capillaries in *Foxf2*$^{-/-}$ brains were thick walled with narrow lumina (Figures 2A–2C); the average ratio of luminal to vessel circumference was 0.46, compared with 0.82 in wild-type ($p < 10^{-7}$; Figure 2C). Confocal cross sections from *mTmG;Wnt1-Cre* brains revealed that an increased investment with neural crest-derived (EGFP+) mural cells was partly responsible for the increased capillary wall thickness (Figure 2B). Transmission electron microscopy (TEM)

(G–L) Anti-Foxf2 (brown) and isolectin (blue) staining of cerebral cortex (G–J) and extra-neuronal (head mesenchyme) blood vessels (K and L) from wild-type (G, I, and K) and *Foxf2*$^{-/-}$ (H, J, and L) E12.5 embryos (G and H: 40×; I–L: 100×). Dashed lines in (G) and (H) indicate boundaries between meninges and brain parenchyma.

(M–P) Anti-Foxf2 (brown) staining of *Foxs1*$^{lacZ/+}$, E12.5, forebrain sections (O and P are magnifications of M and N). Foxf2 is localized to nuclei of *lacZ*+ (blue) neural crest cells in perineural mesenchyme (O) and in brain (insets in M and N) of *Foxf2*$^{+/+}$ (M and O) but not *Foxf2*$^{-/-}$ (N and P) embryos.

(Q) Co-staining with anti-Foxf2 (DAB; brown) and anti-Pdgfrβ (red fluorescence) in E12.5 telencephalon. Erythrocyte (RBC) autofluorescence in green is used to visualize capillaries.

(R) Co-staining with anti-Foxf2 (DAB; brown) and anti-Lef1 (red fluorescence) in E12.5 telencephalon. Erythrocyte (RBC) autofluorescence in green is used to visualize capillaries.

See also Figure S1.

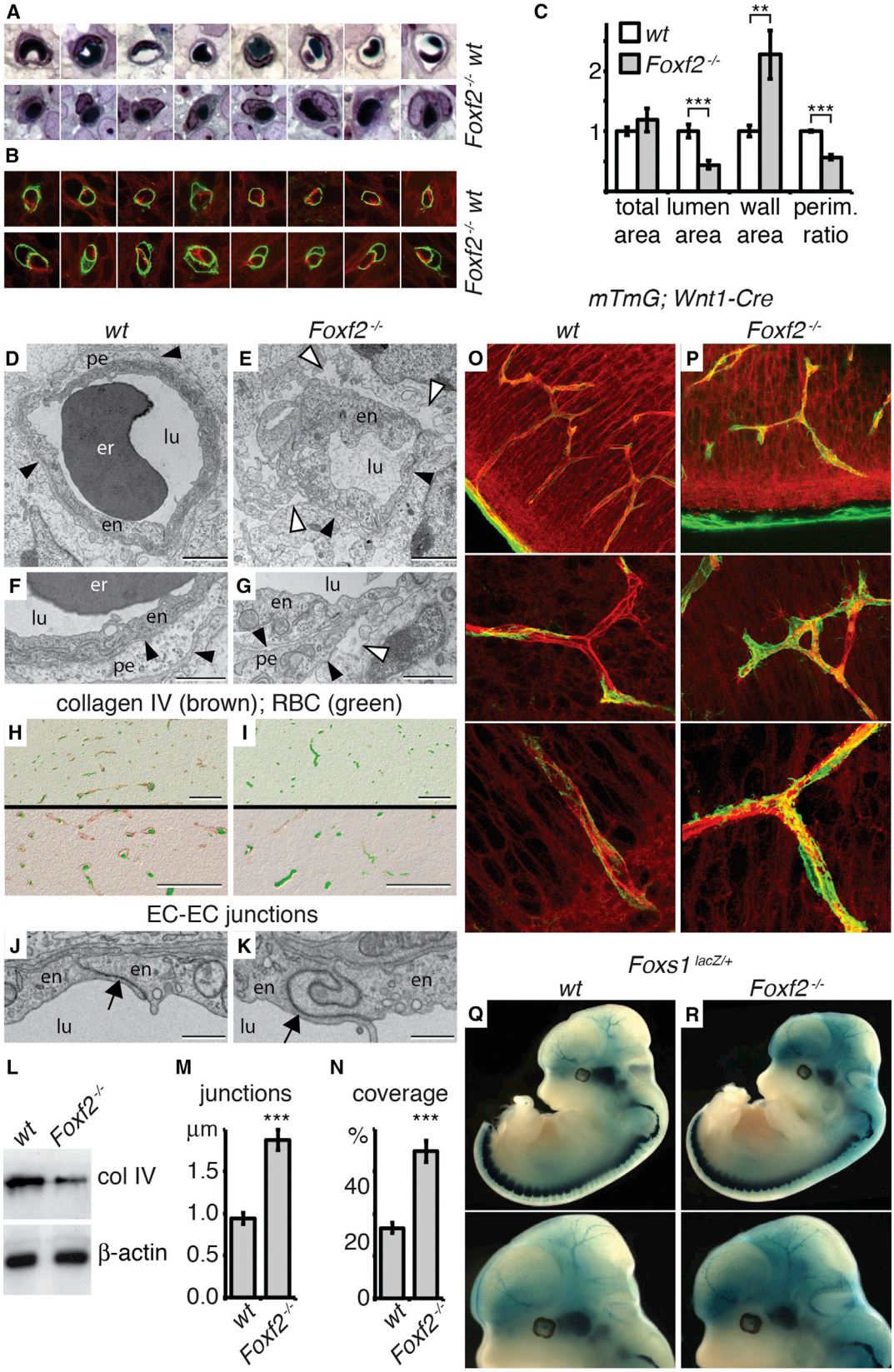

(legend on next page)

showed a thickened and irregular endothelium in *Foxf2*$^{-/-}$ capillaries (Figures 2D, 2E, and S2B), with the immature appearance typical of growing vascular sprouts, rich in cytoplasm and mitochondria (Figures 2E and S2B). In normal capillaries, the basal lamina that surrounds endothelium and pericytes appears as an electron-dense layer of extracellular matrix between, and in close contact with, cells of the neurovascular unit (Figures 2D and 2F). In *Foxf2*$^{-/-}$ brain, the basal lamina was highly variable: normal in some regions but often thin, less electron dense, and in some areas appeared to be missing altogether (Figures 2E, 2G, and S2B). In its place, dilated extracellular spaces surrounded the capillaries, indicative of perivascular edema (Figures 2E, 2G, and S2B). Immunohistochemistry (IHC; Figures 2H and 2I) and western blot (Figure 2L) confirmed reduced amounts of collagen IV around cerebral blood vessels in *Foxf2*$^{-/-}$, whereas the meningeal vasculature had a normal level (Figure S2E). Direct signs of defective tissue integrity in *Foxf2*$^{-/-}$ brains included an elevated sensitivity to the stress inflicted by fixation and tissue processing (Figure S2D) and an extremely rapid equilibration during sucrose infusion prior to cryosectioning.

Junction complexes between capillary endothelial cells were, on average, twice as long and more convoluted in *Foxf2*$^{-/-}$, compared with wild-type (Figures 2J, 2K, 2M, and S2C; $p < 10^{-8}$; n = 40 wild-type and 34 *Foxf2*$^{-/-}$). This may, however, be an inevitable consequence of the thicker and more irregular endothelial cells rather than an independent trait.

Brain Pericyte Number Correlates Negatively with *Foxf2* Gene Dosage

The fraction of the capillary endothelial surface covered by pericytes in *Foxf2*$^{-/-}$ brains was approximately twice that in wild-type, as judged from E18.5 *mTmG*;*Wnt1-Cre* (Figures 2N–2P; 69% versus 33%; $p = 10^{-4}$). Larger blood vessels were not studied systematically, but a cursory examination suggested a corresponding increase in mural cell investment (Figure S2F).

X-gal staining of *Foxs1*^{lacZ} embryos showed an increased density of β-gal+ cells associated with cerebral blood vessels in *Foxf2*$^{-/-}$, without alterations in other neural crest populations (Figures 2Q and 2R). The impact of *Foxf2* gene dosage on mural cell density in different parts of the brain was quantified at several developmental stages from sections of *Foxs1*^{lacZ} embryos (Figures 3A–3H and S3A and S3B). At E11.5, the number of intracerebral β-gal+ cells was few and the difference between *Foxf2*$^{-/-}$ and wild-type was not statistically significant, although the mutants had on average 4-fold more *Foxs1*+ cells (Figure S3A). One day later, E12.5, *Foxf2*$^{-/-}$ brains had 4.5-fold more β-gal+ cells (Figures 3A–3C; $p = 10^{-3}$), and at E18.5, the difference was 1.9-fold (Figure 3H; $p < 10^{-6}$). We also analyzed the *Tg(FOXF2)* transgenic strain, which carries a single-copy insertion of a BAC clone containing the human *FOXF2* gene and 115 kb of flanking sequence (Nik et al., 2013). This transgene, which can rescue the lethal *Foxf2*$^{-/-}$ phenotype, induces an overexpression of *FoxF2* of approximately 50% (in intestinal mesenchyme; Nik et al., 2013). Strikingly, the β-gal+ cell density depended almost linearly on *Foxf2* gene dosage (ANOVA $p < 10^{-12}$) in mutants with both higher and lower than normal allele number: E18.5 *Tg(FOXF2)* had 68% of the wild-type density ($p < 10^{-3}$), heterozygotes were intermediate between wild-type and *Foxf2*$^{-/-}$, and *Foxf2*$^{-/-}$ rescued by *Tg(FOXF2)* was comparable with *Foxf2*$^{-/+}$ (144% and 137%, respectively; Figure 3H). At all developmental stages, the difference in *Foxs1*+ cell density between *Foxf2*$^{-/-}$ and wild-type was similar along the rostrocaudal axis of the brain (Figure S3A), consistent with the higher count in the knockout representing an increase in cell number, rather than faster migration leading to more rapid colonization of the anterior brain vasculature.

Increased Proliferation and Defective Differentiation of *Foxf2*$^{-/-}$ Pericytes

The increased density of cerebral vascular mural cells in response to *Foxf2* inactivation suggested that Foxf2 negatively regulates their proliferation. To address this, we exposed females pregnant with *Foxs1*$^{lacZ/+}$ litters to a BrdU pulse and compared the fraction of intra-cerebral β-gal+ cells that were BrdU+ between *Foxf2*$^{-/-}$ and wild-type littermates (Figures 3I–3K and S3C). At E12.5, *Foxf2* inactivation increased BrdU+ cells from 23% in wild-type to 32% in *Foxf2*$^{-/-}$ ($p = 0.002$) and at E18.5 from 28% to 41% ($p = 0.002$). A similar result was obtained

Figure 2. Cerebrovascular Histology and Ultrastructure of *Foxf2*$^{-/-}$ Embryos

(A) Cross sections of capillaries in the cerebral cortex of E18.5 wild-type (top) and *Foxf2*$^{-/-}$ (bottom) mice.

(B) Cross sections of capillaries in the cerebral cortex of E18.5 wild-type (top) and *Foxf2*$^{-/-}$ (bottom) mice on *mTmG*;*Wnt1-Cre* background. Membranes of neural crest-derived vascular mural cells are green, endothelial membranes bright red, and other cells dull red.

(C) Cross section morphometry of E18.5 cerebral cortex capillaries from wild-type and *Foxf2*$^{-/-}$ mice, showing smaller lumina ($p < 10^{-3}$), thicker vascular walls ($p < 10^{-2}$), and smaller ratio of luminal to outer perimeter ($p < 10^{-7}$) in *Foxf2*$^{-/-}$ capillaries. Error bars = SEM, n = 8 per genotype.

(D–G) TEM of cross sections of E18.5 cortical capillaries showing thickened endothelium (en), shrunken lumen (lu), poorly developed basal lamina (black arrowheads), and gaps of extracellular space (white arrowheads) in *Foxf2*$^{-/-}$ (E and G). er, erythrocyte; pe, pericyte. The scale bars represent 2 μm (D and E) and 1 μm (F and G). For additional examples of *Foxf2*$^{-/-}$ capillaries, see Figure S2B.

(H and I) Anti-collagen IV IHC (brown) of E18.5 cerebral cortex from wild-type (H) and *Foxf2*$^{-/-}$ (I) mice at 20× (top) and 40× (bottom). Erythrocyte autofluorescence (green) is used to visualize capillaries. For additional collagen IV IHC, see Figure S2E.

(J and K) Inter-endothelial junctions (black arrows) in wild-type (J) and *Foxf2*$^{-/-}$ capillaries (K). The scale bars represent 0.5 μm. For additional examples of EC-EC junctions, see Figure S2C.

(L) Collagen IV western blot (β-actin as loading control) of E18.5 wild-type and *Foxf2*$^{-/-}$ brains.

(M) Average lengths of inter-endothelial junctions in cross sections of wild-type and *Foxf2*$^{-/-}$ capillaries. $p < 10^{-8}$; n = 40 wild-type and 34 *Foxf2*$^{-/-}$. Error bars = SEM.

(N) Pericyte coverage of forebrain capillaries based on confocal images of E18.5 *mTmG*;*Wnt1-Cre* brains. $p = 10^{-4}$; n = 6 per genotype; error bars = SEM.

(O and P) Cerebral cortex capillaries at three different magnifications from E18.5 *mTmG*;*Wnt1-Cre*, wild-type and *Foxf2*$^{-/-}$ mice. Pericytes are green, endothelium bright red, and other cells dull red.

(Q and R) Distribution and abundance of neural crest cells visualized by *Foxs1*^{lacZ} (blue) in E12.5 wild-type and *Foxf2*$^{-/-}$ embryos.

See also Figure S2.

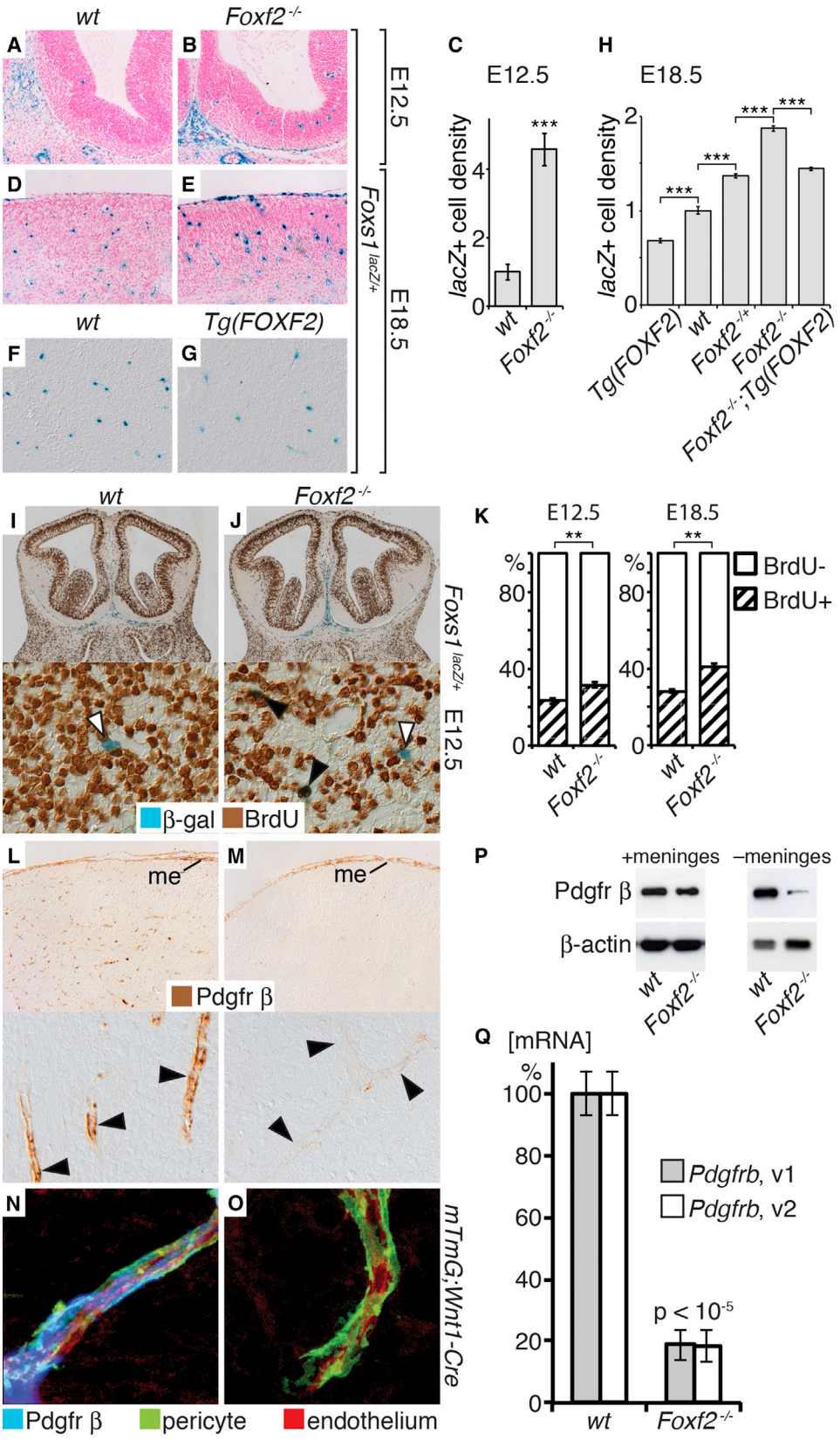

(legend on next page)

with the proliferation marker PCNA at E18.5 (Figures S3D and S3E; $p < 10^{-3}$; 19% $PCNA^+$ in wild-type versus 42% in *Foxf2*$^{-/-}$). Elevated proliferation can thus account for the increased pericyte density in *Foxf2*$^{-/-}$ brain.

Next, we investigated how *Foxf2* deletion affected brain pericyte differentiation. IHC with anti-Pdgfrβ on *Foxf2*$^{-/-}$ E18.5 brain showed a normal pattern in the meningeal vasculature but very weak staining of the capillaries in the brain parenchyma (Figures 3L and 3M). On *mTmG;Wnt1-Cre* background, anti-Pdgfrβ co-stained with the green fluorescence of brain pericytes in wild-type but was barely detectable in the *Foxf2*$^{-/-}$ mutant (Figures 3N and 3O). Western blot with brain extracts that included the meninges showed a moderate decrease of Pdgfrβ in the *Foxf2* mutant (66 ± 12% of wild-type), whereas in samples in which the meninges had been removed, the difference was more pronounced (*Foxf2*$^{-/-}$ 17 ± 3% of wild-type; Figure 3P). qPCR indicated that *Foxf2*$^{-/-}$ brain (without meninges) had less than 20% of the wild-type level of *Pdgfrb* mRNA, in spite of possession of almost twice the number of pericytes (Figure 3Q; $p < 10^{-5}$). Other pericyte markers were less affected; Tem1 was present at 69 ± 9% of wild-type level (Figure S3F), whereas the amount of Ng2 was unaltered (Figure S3G) in extracts of *Foxf2*$^{-/-}$ brains. Expression of desmin was delayed in the *Foxf2* mutant; at E13.5, anti-desmin staining of brain capillaries was significantly weaker in *Foxf2*$^{-/-}$ than in wild-type, whereas the E18.5 patterns were comparable (Figure S3H).

Intracranial Hemorrhage and Defective BBB in *Foxf2*$^{-/-}$ Embryos

From E12.5, many *Foxf2*$^{-/-}$ embryos exhibited variable degrees of intracranial hemorrhage (ICH; Figures 4A and 4B), and TEM revealed microbleeds in the form of scattered extravascular erythrocytes in the brain parenchyma (Figure S4A).

To assess the integrity of the BBB, we used intraperitoneal injections of the tracer Evans blue on E18.5 fetuses in utero. Evans blue binds avidly to serum albumin, and its accumulation in the brain indicates albumin leakage from the vasculature due to breakdown of the BBB (Hawkins and Egleton, 2006). Three hours after injection, *Foxf2*$^{-/-}$ brains had widespread blue staining (Figure 4D). The distribution and intensity varied among individuals but were in all cases clearly distinguishable from the unstained brains of wild-type littermates (Figure 4C). On average, *Foxf2*$^{-/-}$ brains held 224% of the amount of Evans blue retained in wild-type, on the basis of spectrophotometric quantification of whole brain extracts (Figure 4E; $p < 10^{-4}$), and were 10% heavier, suggestive of cerebral edema, but the latter difference was not statistically significant (p = 0.07).

Decreased Tgfβ Signaling in *Foxf2*$^{-/-}$ Brain Vasculature

Tgfβ signaling is essential for many aspects of vascular development, including differentiation of endothelial and mural cells and production of the extracellular matrix of the vascular basal lamina (Gaengel et al., 2009). Inhibition of this pathway by targeting *Smad4* in cerebrovascular endothelial cells caused defects similar to the *Foxf2*$^{-/-}$ phenotype described here, including ICH and BBB breakdown (Li et al., 2011). We therefore compared canonical Tgfβ signaling, measured as Smad2/3 phosphorylation (P-Smad2/3), in E18.5 *Foxf2*$^{-/-}$ and wild-type brains. The amount of Smad2/3 protein was not altered, but the level of P-Smad2/3 was significantly reduced in the mutant (Figures 4F and 4G). IHC with phospho-specific anti-P-Smad2/3 showed activated Smad2/3 to be associated with capillaries, to be less abundant in the *Foxf2* mutant, and not detected in *Foxs1*^{lacZ}-positive pericytes (Figure 4F). Cell-type-specific loss-of-function phenotypes indicate that the Alk5-Smad2/3 pathway is active in endothelial cells and vSMCs, whereas the status in pericytes is disputed (reviewed by Gaengel et al., 2009). Our inability to detect P-Smad2/3 in *Foxs1*^{lacZ}+ pericytes of either genotype (Figure 4F) may be due to limitations in sensitivity but suggests that the concentration in endothelial cells is significantly higher.

The amounts of the Tgfβ ligand Tgfβ2, the type 2 receptor Tgfβr2, and the type 1 receptor Alk5 were all reduced in *Foxf2*$^{-/-}$ brain, at the protein and/or mRNA level (Figures 4G and 4H), whereas the levels of Tgfβ1, Tgfβ3, and Tgfβr3 were normal (Figures S4B and S4C). Tgfβ signaling through Alk5 and Smad2/3 has an antagonistic relationship to the Alk1-Smad1/5 pathway (Goumans et al., 2002), as well as to the non-canonical pathway mediated by p38 (Iwata et al., 2012). Consistent with the reduction in P-Smad2/3, phosphorylation of both Smad1/5 and p38 were increased in *Foxf2* mutant brain (Figure 4G). No change in expression of the Smad phosphatase Ppm1a was

Figure 3. Increased Proliferation and Defective Differentiation of Brain Pericytes in *Foxf2*$^{-/-}$ Embryonic Brain

(A and B) Sections of E12.5 telencephalon with perineural mesenchyme from X-gal stained wild-type (WT) (A) and *Foxf2*$^{-/-}$ (B) embryos on *Foxs1*$^{lacZ/+}$ background.

(C) Relative density of β-gal+ nuclei in brains of E12.5 wild-type and *Foxf2*$^{-/-}$ embryos on *Foxs1*$^{lacZ/+}$ background. $p = 10^{-3}$, n = 3 per genotype.

(D–G) Sections of E18.5 cerebral cortex from X-gal stained wild-type (D and F), *Foxf2*$^{-/-}$ (E) and Tg(*FOXF2*) (G) embryos on *Foxs1*$^{lacZ/+}$ background.

(H) Relative density of β-gal+ nuclei in brains of E18.5 mice with different *Foxf2* genotype. $p < 10^{-3}$ (*Tg(FOXF2)* versus WT), $p < 10^{-4}$ (*Foxf2*$^{-/+}$ versus WT), $p < 10^{-4}$ (*Foxf2*$^{-/+}$ versus *Foxf2*$^{-/-}$), $p < 10^{-6}$ (*Foxf2*$^{-/-}$ versus WT), $p < 10^{-3}$ (*Foxf2*$^{-/-}$;*Tg[FOXF2]* versus *Foxf2*$^{-/-}$). n = 8 WT, 4 *Tg[FOXF2]*, 5 *Foxf2*$^{-/+}$, 3 *Foxf2*$^{-/-}$, 3 *Foxf2*$^{-/-}$;*Tg[FOXF2]*.

(I and J) BrdU (brown) labeling of S-phase nuclei in E12.5 wild-type (I) and *Foxf2*$^{-/-}$ (J) embryos on *Foxs1*$^{lacZ/+}$ background. Arrowheads indicate β-gal+ (blue) nuclei; white for BrdU– and black for BrdU+.

(K) Fraction of β-gal+ nuclei in brain that are BrdU+ at E12.5 (left) and E18.5 (right) in wild-type and *Foxf2*$^{-/-}$ on *Foxs1*$^{lacZ/+}$ background (E12.5: 23% BrdU+ in wild-type versus 32% in *Foxf2*$^{-/-}$, p = 0.002, n = 7 per genotype; E18.5: 28% BrdU+ in wild-type versus 41% in *Foxf2*$^{-/-}$, p = 0.002, n = 3 per genotype).

(L and M) Anti-Pdgfrβ IHC on sections of cerebral cortex from wild-type (L) and *Foxf2*$^{-/-}$ (M) E18.5 brains at high and low magnification. Arrowheads indicate capillaries. me = meninges.

(N and O) Anti-Pdgfrβ IF (blue) on cerebral cortex capillaries from wild-type (N) and *Foxf2*$^{-/-}$ (O) E18.5 *mTmG;Wnt1-Cre* mice. Pericytes are green, endothelium bright red, and other cells dull red.

(P) Pdgfrβ western blots (β-actin as loading control) with extracts made from E18.5 brains (wild-type and *Foxf2*$^{-/-}$) with or without meninges.

(Q) *Pdgfrb* mRNA (two splice versions; by qPCR) in E18.5 wild-type and *Foxf2*$^{-/-}$ brain (meninges removed; $p < 10^{-5}$; n = 6 per genotype).

Error bars in (C), (H), (K), and (Q) = SEM. See also Figure S3.

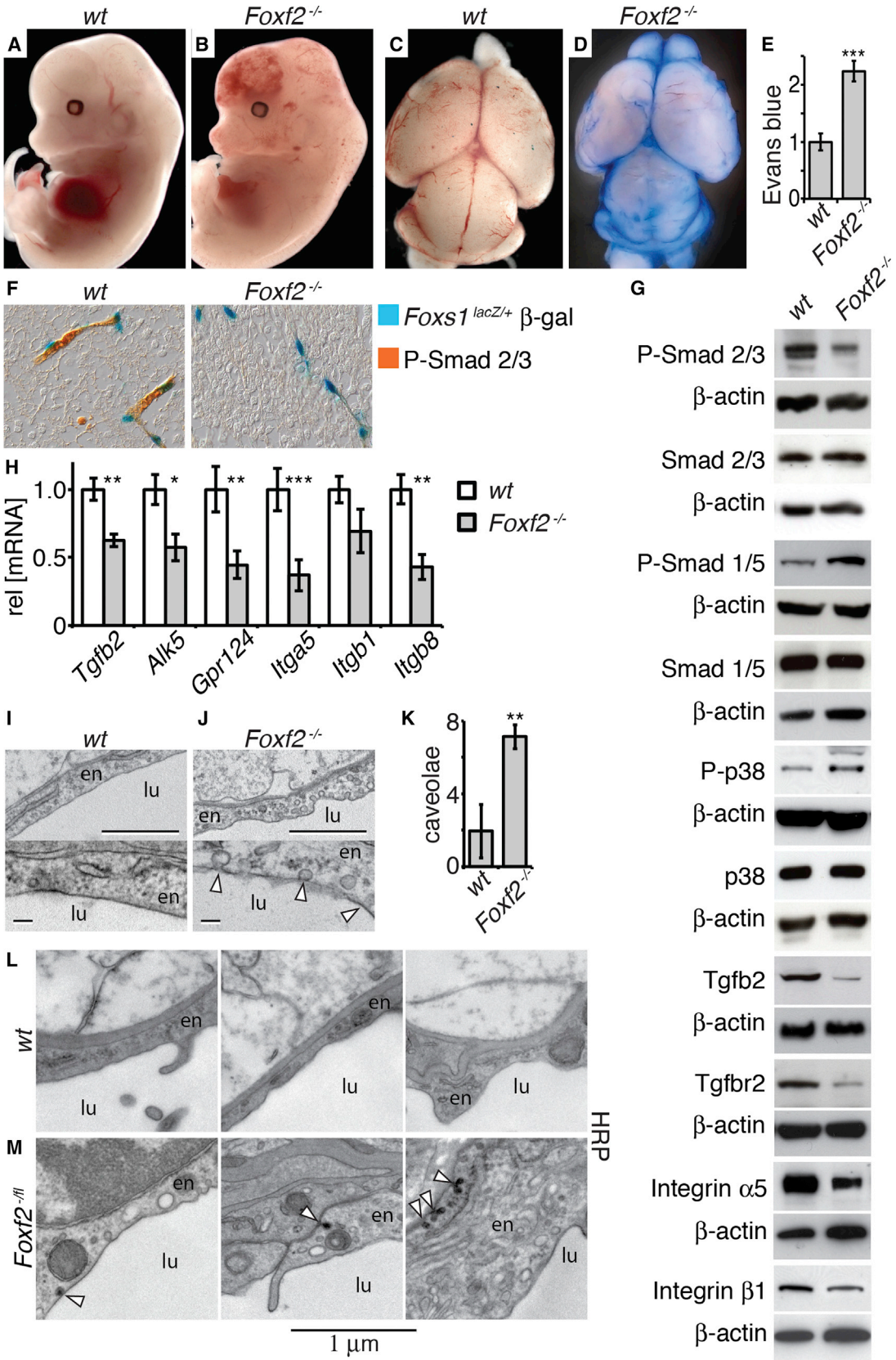

(legend on next page)

detected (Figure S4B), which is compatible with the reduction in P-Smad2/3 being the result of decreased phosphorylation, rather than increased de-phosphorylation, and fits the notion of diminished signaling by Alk5/Tgfβr2.

Integrins are important for activation of latent extracellular Tgfβ complexes, and genetic ablation of integrin α_V or β_8 causes defective angiogenesis associated with attenuated Tgfβ signaling (Arnold et al., 2014; Bader et al., 1998; Cambier et al., 2005; Zhu et al., 2002). qPCR showed significantly reduced mRNA levels for both chains of the dominating integrin in CNS vasculature, $\alpha_V\beta_8$ (Figure 4H; *Itga5*, 32% of wild-type, $p < 0.001$; Itgb8, 43% of wild-type, $p = 0.002$). Integrin α_V protein level was reduced correspondingly (Figure 4G), and integrin β_1 also showed a modest reduction of both mRNA and protein (Figures 4G and 4H).

The G protein-coupled receptor Gpr124 is both a target and a regulator of Tgfβ signaling; *Gpr124*-knockout mice have cerebrovascular defects associated with perturbed Tgfβ pathway activation, and Tgfβ increases *Gpr124* expression (Anderson et al., 2011). Consistent with the diminished Smad2/3 phosphorylation, *Gpr124* mRNA in *Foxf2*$^{-/-}$ brains was reduced to less than half the wild-type level (Figure 4H; $p = 0.01$).

mRNA for other proteins known to be important in angiogenesis, or cross-talk between pericytes and endothelial cells, such as angiopoietins 1 and 2 (*Angpt1*, *Angpt2*), vascular endothelial growth factor A (*Vegfa*), and connexins 43 and 45 (*Gja1*, *Gjc1*), was not significantly altered in the *Foxf2* mutant brain (Figure S4B). Neither was the mRNA level for *Foxc1* (Figure S4B), a related forkhead gene located 175 kb from *Foxf2*, which is expressed in the brain vasculature and important for its development (Siegenthaler et al., 2013).

The tight association between astrocytes and the vasculature does not develop until postnatally (Daneman et al., 2010), but already at E18.5 aquaporin 4, an astrocyte marker, is enriched along brain capillaries (Figures S4D and S4E). In *Foxf2*$^{-/-}$ brains, aquaporin 4 staining was diffuse and not obviously associated with the vasculature, although the amount of protein (Figure S4C) and mRNA (97 ± 12% of wild-type; n = 14 per genotype) was normal.

Increased Trans-endothelial Vesicular Transport in *Foxf2*$^{-/-}$ Brains

Endothelial cells of *Foxf2*$^{-/-}$ brain capillaries contained abundant cytoplasmic vesicles, which suggested increased vesicle mediated trans-cytosis, and high magnification of the luminal endothelial membrane revealed an increased density of caveolae (Figures 4I–4K and S4F; 7.13/capillary in *Foxf2*$^{-/-}$ versus 1.95 in wild-type; $p < 0.01$).

To investigate if these vesicles transported luminal content across the endothelium required a tracer observable by TEM and the ability to do experiments in postnatal mice. We generated a conditional allele of *Foxf2* (*Foxf2*^{fl}; Figure S4G) in which *loxP* sites flank the first exon, and combined it with inducible *CAGG-Cre*^{ERT2} (Hayashi and McMahon, 2002). Inactivation of *Foxf2* in adult *Foxf2*$^{fl/-}$ and *Foxf2*$^{fl/fl}$ mice by tamoxifen led to a gradual increase in brain vascular permeability (see next section). Intravenous injection with horseradish peroxidase (HRP) 15 min before euthanasia and perfusion fixation, followed by diaminobenzidine (DAB) staining and TEM, showed DAB precipitates in caveolae and vesicles of *Foxf2*$^{fl/-}$ endothelial cells (Figure 4M). The occurrence of DAB+ vesicles next to the abluminal membrane indicated trans-endothelial transport of HRP. No accumulation of DAB precipitates was observed in junctions between endothelial cells, which suggests that increased vesicular transport is the principal factor behind the vascular permeability in *Foxf2* mutant brains.

Foxf2 Is Required for Maintained BBB in Adult Mice

The role of pericytes in establishment of the BBB during development has been clearly demonstrated, but their importance for maintenance of vascular integrity has been questioned, and the relative contribution of pericytes and astrocytes for permeability regulation in the adult CNS vasculature remains unclear (Armulik et al., 2010; Daneman et al., 2010). We therefore asked whether persistent *Foxf2* expression is required to uphold BBB integrity, or if it is dispensable once the vasculature has matured.

Conditional knockouts (*Foxf2*$^{fl/fl}$ and *Foxf2*$^{fl/-}$) responded to tamoxifen-induced *Foxf2* deletion with weight loss, rapid during the first month and then more slowly (Figure S5A). The mortality of *Foxf2*$^{fl/fl}$ was 40% during the first 6 weeks after Cre induction, whereas all other genotypes, including *Foxf2*$^{fl/-}$, had normal survival. BBB integrity was not significantly affected during the first 3 weeks after *Foxf2* deletion. However, after 6 weeks, the average Evans blue retention in *Foxf2*$^{fl/-}$ brains was >4-fold higher than in wild-type, *Foxf2*$^{fl/+}$ ($p < 10^{-10}$), or heterozygotes ($p < 10^{-6}$), and the mutant brains turned distinctly blue (Figures 5A, 5B, S5B, and S6). Surprisingly, *Foxf2*$^{fl/fl}$ brains had even

Figure 4. *Foxf2*$^{-/-}$ Brains Have a Leaky BBB and Reduced Tgfβ Signaling

(A and B) ICH in E13.5 *Foxf2*$^{-/-}$ (B) embryo, with wild-type littermate (A) for comparison.

(C and D) Evans blue leakage into E18.5 *Foxf2*$^{-/-}$ (D), but not wild-type (C), brain.

(E) Quantification of Evans blue in E18.5 brains. *Foxf2*$^{-/-}$ brains contained on average 2.24-fold more Evans blue than wild-type; $p < 10^{-4}$, n = 9 *Foxf2*$^{-/-}$ and 12 wild-type.

(F) Anti-phospho-Smad2/3 IHC (brown) and X-gal staining (blue) of sections of cerebral cortex from E18.5 wild-type and *Foxf2*$^{-/-}$ mice on *Foxs1*$^{lacZ/+}$ background.

(G) Western blots with brain extracts from E18.5 wild-type and *Foxf2*$^{-/-}$ mice.

(H) mRNA (by qPCR) for proteins involved in Tgfβ signaling in E18.5 *Foxf2*$^{-/-}$ brain (as percentage of wild-type): *Tgfb2* 60%, $p = 0.002$; *Alk5* 57%, $p < 0.02$; *Gpr124* 45%, $p = 0.01$; *Itga5* 32%, $p < 0.001$; *Itgb1* 69%, $p = 0.1$; *Itgb8* 43%, $p = 0.002$; n = 6 per genotype.

(I and J) Low (top) and high (bottom) magnification TEM images of brain capillary endothelium showing more luminal caveolae (arrowheads) in *Foxf2*$^{-/-}$ mutants (J) than in wild-type (I). The scale bars represent 1 μm (top) and 100 nm (bottom).

(K) Number of luminal caveolae (average 1.95/capillary in wild-type versus 7.13 in *Foxf2*$^{-/-}$; n = 8 per genotype; $p < 0.01$).

(L and M) TEM images of DAB-stained brain tissue from adult wild-type (L) and *Foxf2*$^{-/fl}$;*CAGG-Cre* (M) mice injected with HRP 15 min before perfusion. The endothelial cells of *Foxf2*$^{-/fl}$ mutants have DAB+ caveolae and vesicles (arrowheads) present on both luminal (left image) and abluminal (right image) sides.

Error bars in (E), (H), and (K) = SEM. See also Figure S4.

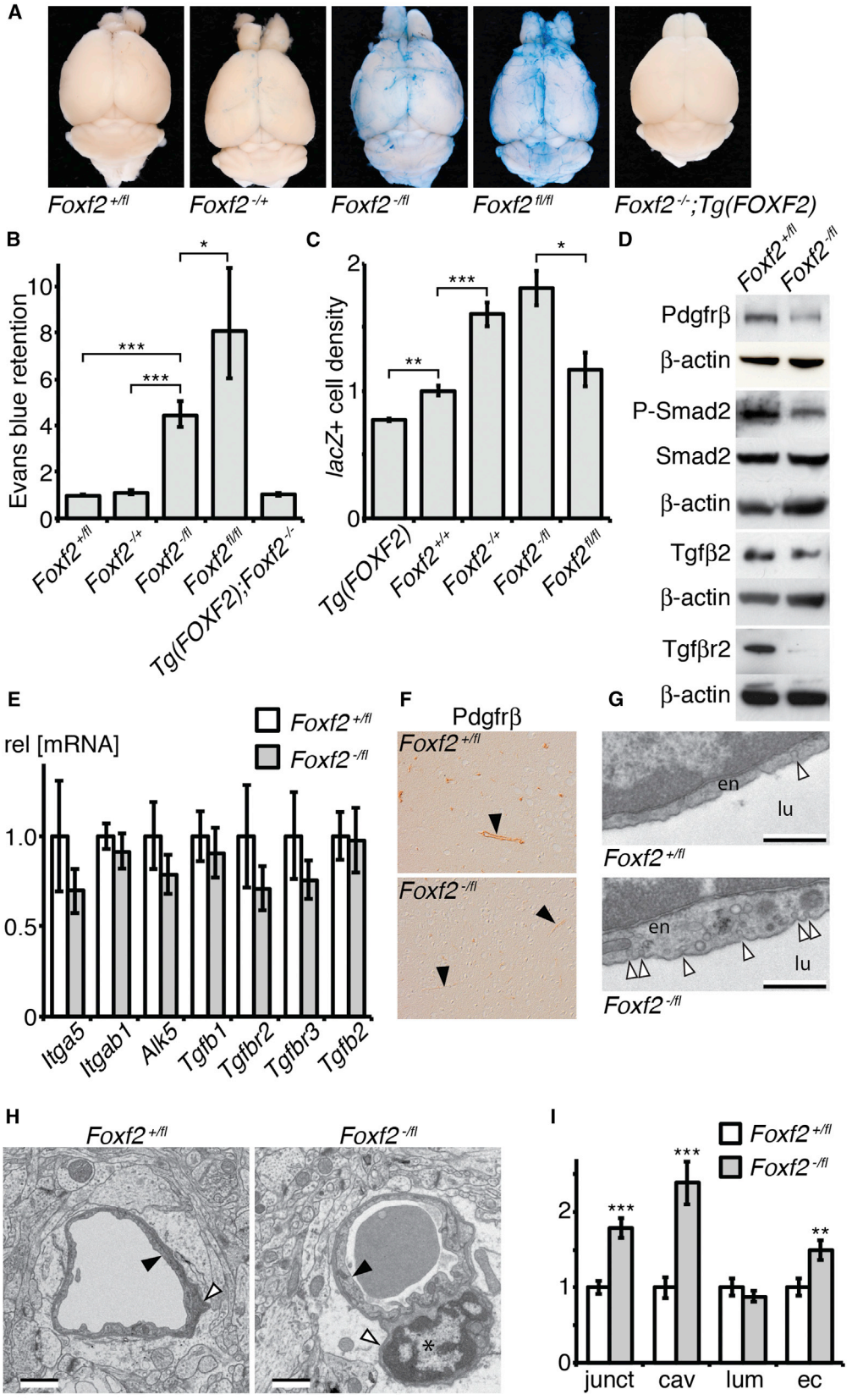

(legend on next page)

more damaged barrier function and held on average 8-fold more tracer than *Foxf2*$^{fl/+}$ (Figures 5A and 5B; $p < 10^{-8}$ versus *Foxf2*$^{fl/+}$ and $p < 0.05$ versus *Foxf2*$^{fl/-}$). Neither *Foxf2*$^{-/+}$ heterozygotes (111%) nor knockout mice rescued by the *Tg(FOXF2)* transgene (*Foxf2*$^{-/-}$;*Tg[FOXF2]*; 104%) differed significantly from wild-type or *Foxf2*$^{fl/+}$ (100%).

Differences in pericyte number, measured as β-gal+ cell density in *Foxs1*$^{lacZ/+}$ cerebral cortex, as a function of *Foxf2* gene dosage was similar in adult mice to that of E18.5: *Tg(FOXF2)* had less (77%; $p < 10^{-2}$) and *Foxf2*$^{-/+}$ more (160%; $p < 10^{-4}$) than wild-type (100%; Figure 5C). No dramatic increase in pericyte density occurred in response to *Foxf2* inactivation in adults: after 6 weeks, *Foxf2*$^{fl/fl}$ did not differ significantly from wild-type (117% versus 100%; $p = 0.12$) and *Foxf2*$^{fl/-}$ not from *Foxf2*$^{-/+}$ (181% versus 160%; $p = 0.22$; Figure 5C). The negative correlation between pericyte density and *Foxf2* gene dosage is thus established during development and is not or little affected by *Foxf2* inactivation in adulthood. The difference in pericyte number between *Foxf2*$^{fl/-}$ and *Foxf2*$^{fl/fl}$ presents a possible explanation for why the latter suffered higher mortality and leakier BBB, even though *Foxf2* loss is expected to be more complete in the former. During development, *Foxf2*$^{fl/-}$ establishes a significantly higher pericyte density than *Foxf2*$^{fl/fl}$, which may partially protect against defective pericyte function later on when *Foxf2* is deleted.

The reduced number of pericytes in *Tg(FOXF2)*, with three functional copies of the gene, confirms that the negative correlation between *Foxf2* allele number and density of cerebral pericytes is evident at all ages, embryonic and adult, and in animals with both increased and decreased gene dosage. Interestingly, but consistent with the correlation between pericyte coverage and vascular permeability, *Tg(FOXF2)* brains had a modest (60%) but highly reproducible ($p < 10^{-3}$) increase in Evans blue permeability (Figure S5C).

Foxf2 inactivation in adults had a similar effect on Pdgfrβ as in embryos, with reduced immunoreactivity of cortical capillaries (Figures 5D and 5F) but persistent expression level in meninges (Figure S5D). In contrast, no alteration in desmin, *Vegfa*, or aquaporin 4 was observed (Figures S5E–S5G). Smad2 level was not affected, but its phosphorylation was reduced, as was the level of Tgfβr2 (Figure 5D). mRNA quantifications suffered from inter-individual variation, and none of the genes involved in Tgfβ signaling showed a significant difference. The trend, however, was the same as in *Foxf2*$^{-/-}$ embryos, with less mRNA for *Itga5*, *Alk5*, and *Tgfbr2* (Figure 5E).

TEM analysis of cortical capillaries revealed that *Foxf2* inactivation resulted in a 2.4-fold increase in luminal caveolae (Figures 5G and 5I; $p < 10^{-4}$), lengthening of inter-endothelial junctions (Figure 5I; $p < 10^{-5}$), and a thickening of the endothelium by approximately 50% (Figures 5H and 5I; $p < 0.01$; $n = 50$ cross sections per genotype). No significant differences were observed in capillary density (Figure S5H) or in overall vessel dimensions or shape parameters (Figure S5I). We also scored the sections for the presence or absence of pericyte nuclei and noted a doubling of the frequency, from 5.7% in *Foxf2*$^{fl/+}$ to 12.2% in *Foxf2*$^{fl/-}$ ($p < 0.05$; $n = 141$ *Foxf2*$^{fl/+}$ cross sections and 131 *Foxf2*$^{fl/-}$). The higher frequency of pericyte nuclei is consistent with the 1.8-fold increase in β-gal+ cells in *Foxf2*$^{fl/-}$;*Foxs1*$^{lacZ/+}$ (Figure 5C).

Taken together, these results demonstrate that persistent *Foxf2* expression is required to maintain the barrier function in the mature cerebral vasculature. Adult inactivation of *Foxf2* did not cause the severe structural defects observed as a result of *Foxf2* deficiency during development but increased vascular permeability significantly.

DISCUSSION

The next neighbor of *FoxF2* in the genomes of mice and man—*FoxC1*, encoding another forkhead transcription factor and located approximately 200 kb downstream of *FoxF2*—is expressed in the brain vasculature and influences vessel morphogenesis and proteoglycan expression (Siegenthaler et al., 2013). *Foxc1* inactivation did not affect the BBB, Pdgfrβ, or Tgfβ signaling (Siegenthaler et al., 2013) and is therefore mechanistically distinct from that of *Foxf2*. Murine *Foxc1* mutants had increased proliferation of both endothelial cells and pericytes, whereas *FoxC1* knockdown in zebrafish was reported to impair recruitment of mural cells and neural crest migration (French et al., 2014). Deletion of *Foxf2* did not affect expression of *Foxc1*; a transgenic strain with increased *FoxF2* gene dosage, *Tg(FOXF2)*, has a phenotype opposite that of the *Foxf2* knockout; and transgenic rescue of *Foxf2*$^{-/-}$ by *Tg(FOXF2)* produced a phenotype indistinguishable from the heterozygote.

Figure 5. BBB Breakdown upon Inactivation of *Foxf2* in Adult Mice

(A and B) Images (A) and quantification (B) of Evans blue retention in brains of mice with different *Foxf2* genotype. $p < 10^{-10}$ (*Foxf2*$^{-/fl}$ versus *Foxf2*$^{+/fl}$); $p < 10^{-6}$ (*Foxf2*$^{-/fl}$ versus *Foxf2*$^{-/+}$); $p < 0.05$ (*Foxf2*$^{-/fl}$ versus *Foxf2*$^{fl/fl}$); $p < 10^{-4}$ (*Foxf2*$^{-/fl}$ versus *Tg[FOXF2];Foxf2*$^{-/-}$). *Foxf2*$^{-/+}$ (111%) and *Tg(FOXF2);Foxf2*$^{-/-}$ (104%) not significantly different from *Foxf2*$^{+/fl}$ (100%). $n = 12$ *Foxf2*$^{-/+}$, 8 *Foxf2*$^{-/+}$, 9 *Foxf2*$^{-/fl}$, 5 *Foxf2*$^{fl/fl}$, and 3 *Tg(FOXF2);Foxf2*$^{-/-}$.

(C) Relative density of β-gal+ nuclei in brains of *Foxs1*$^{lacZ/+}$ mice with different *Foxf2* genotype. $p = 0.007$ (*Tg[FOXF2]* versus WT); $p < 10^{-4}$ (*Foxf2*$^{-/+}$ versus WT); $p < 10^{-4}$ (*Foxf2*$^{-/fl}$ versus WT); $p = 0.02$ (*Foxf2*$^{-/fl}$ versus *Foxf2*$^{fl/fl}$); $p = 0.03$ (*Foxf2*$^{-/+}$ versus *Foxf2*$^{fl/fl}$). *Foxf2*$^{-/fl}$ (181%) not significantly different from *Foxf2*$^{-/+}$ (160%), and *Foxf2*$^{fl/fl}$ (117%) not significantly different from WT (*Foxf2*$^{+/+}$, 100%). $n = 3$ *Tg(FOXF2)*, 8 WT, 8 *Foxf2*$^{-/+}$, 7 *Foxf2*$^{-/fl}$, and 3 *Foxf2*$^{fl/fl}$.

(D) Western blots with brain extracts from adult *Foxf2*$^{-/fl}$ and *Foxf2*$^{+/fl}$ mice.

(E) mRNA (by qPCR) for proteins involved in Tgfβ signaling in adult *Foxf2*$^{-/fl}$ brain (as percentage of *Foxf2*$^{+/fl}$); $n = 5$ per genotype.

(F) Anti-Pdgfrβ IHC of cerebral cortex from *Foxf2*$^{-/fl}$ and *Foxf2*$^{+/fl}$ mice. Arrowheads indicate capillaries.

(G) Increased number of luminal caveolae (arrowheads) in brain capillary endothelium of *Foxf2*$^{-/fl}$. The scale bars represent 0.5 μm.

(H) Cross sections of cerebral cortex capillaries from *Foxf2*$^{-/fl}$ and *Foxf2*$^{+/fl}$ mice showing thickening of endothelium (black arrowheads) and increased number of pericyte (white arrowheads) nuclei (asterisk in *Foxf2*$^{-/fl}$). The scale bars represent 1μm.

(I) Inter-endothelial junction length (junct), luminal caveolae density (cav), luminal area (lum), and endothelial cell area (ec) of *Foxf2*$^{-/fl}$ relative to *Foxf2*$^{+/fl}$ quantified from TEM images of capillary cross sections from cerebral cortex ($n = 50$ sections per genotype; $p < 10^{-5}$ for junctions, $p < 10^{-4}$ for caveolae, and $p = 0.005$ for endothelial cell area).

Error bars = SEM in (B) (linear representation of SEM of log values), (C), (E), and (I). See also Figures S5 and S6.

Together, these observations strongly support the notions that deletion of *Foxf2* does not affect *Foxc1*, and the *Foxf2* knockout phenotype is not a result of perturbed *Foxc1* expression.

Foxf2 deficiency increases rather than decreases pericyte density. The mechanism underlying BBB breakdown is therefore qualitatively different from that of Pdgfb/Pdgfrβ mutants and likely to represent a differentiation defect in pericytes that indirectly affects the endothelium. Two of the major paracrine signaling pathways involved in pericyte-endothelial communication are affected: Pdgfb/Pdgfrβ and Tgfβ. Signaling in endothelial cells and pericytes are highly entangled, and perturbations of the Tgfβ pathway tend to result in similar molecular and phenotypical signatures, independent of where the primary defect resides. To aid in mechanistic understanding, work is in progress to identify Foxf2 target genes and to separate endothelial from pericyte gene expression alterations.

The increased pericyte density, in spite of less Pdgfrβ in *Foxf2*$^{-/-}$ mutants, contradicts the firmly established requirement for Pdgfb and its receptor for recruitment of pericytes to the brain vasculature. Because of the residual *Pdgfrb* expression in *Foxf2*$^{-/-}$ brain (estimated to 10%), Pdgfrβ may still be essential for guiding CNS pericyte migration, but the robust mural cell investment throughout the cerebrovascular tree in *Foxf2* mutants suggests that other cues are used. The existence of such alternative mechanisms for pericyte recruitment is illustrated by the Pdgfb/Pdgfrβ independent colonization by hepatic stellate cells (Hellström et al., 1999), and the neural crest-derived pericytes of the thymus (Foster et al., 2008). The requirement for Pdgfrβ signaling for pericyte proliferation is apparently lost in the absence of Foxf2.

Increased pericyte proliferation is consistent with the observed reduction in Smad2/3 phosphorylation and the corresponding increase in P-Smad1/5; Tgfβ signaling through Alk5-Smad2/3 promotes differentiation and inhibits proliferation of both endothelial cells and pericytes, whereas Alk1-Smad1/5 does the opposite (Armulik et al., 2011; Winkler et al., 2011). Other phenotypic traits in *Foxf2* mutants characteristic of attenuated vascular Tgfβ are extracellular matrix deficiency, vascular immaturity, and ICH (Li et al., 2011). The reduced levels of Tgfβ2, Alk5, Tgfβr2, and *Gpr124* are likely to contribute to the weaker signaling, as are decreased amounts of integrins α_V and β_8, which are important for activation of latent Tgfβ (Cambier et al., 2005; Shi et al., 2011; Wipff and Hinz, 2008). *Gpr124* and vascular integrins are also targets of Alk5-Smad2/3, and the lowered expression may therefore both contribute to, and be a consequence of, diminished Smad2/3 phosphorylation. Interestingly, recent data (Arnold et al., 2014) indicate that loss of integrins $\alpha_V\beta_8$ leads to cerebral hemorrhage and vascular dysplasia with intact BBB, whereas *Pdgfb*$^{ret/ret}$ have essentially the opposite phenotype, with BBB disruption, but no hemorrhage. This suggests that in *Foxf2* mutants the diminished Pdgfrβ is responsible for BBB breakdown, whereas reduction in Tgfβ and integrin expression may lead to vascular instability and hemorrhage.

CNS pericytes have been shown to be required for establishment of the BBB during embryonic development at a stage that precedes astrocytic endfeet integration into the neurovascular unit (Daneman et al., 2010). A model has been proposed in which the maintenance of BBB integrity is taken over by the astrocytes as the vasculature matures, leaving the pericytes obsolete (Daneman et al., 2010). Inactivation of *Foxf2* in adult mice led to a gradual increase in vascular permeability over a period of several weeks. The slow kinetics suggests that the link between Foxf2 in pericytes and regulation of endothelial permeability contains components that are turned over slowly and possess a fair amount of buffering capacity, perhaps involving reciprocal signaling between several cell types. However, it is clear that continued presence of properly differentiated pericytes is essential for maintenance of the BBB also in the adult. The histological consequences of Foxf2 deficiency were subtler than during embryonic development, but the endothelium became thicker and vascular permeability increased significantly.

Higher than normal gene dosage of *Foxf2* produced a phenotype that mirrored the loss of function, with decreased brain pericyte density. Whereas loss of function resulted in a leaky vasculature with an excess of defective pericytes, a 50% increase in *FoxF2* gene dosage reduced pericyte density, which led to the expected increase in permeability. Importantly, wild-type *Foxf2* gene dosage provides the tightest brain vasculature.

The sensitivity to altered *Foxf2* expression level suggests that genetic alterations that affect the regulation, or copy number, of the human *FOXF2* gene could predispose to cerebrovascular disease and stroke. Interestingly, several reports have linked white matter abnormalities and stroke to copy-number variations in the relevant chromosomal region, 6p25 (Cellini et al., 2012; Kapoor et al., 2011; Rosenberg et al., 2013; van der Knaap et al., 2006; Vernon et al., 2013). Interpretations are complicated by the fact that *FOXC1* are located only 214 kb downstream (centromeric) of *FOXF2*, and recently genetic variants centromeric of *FOXC1* were associated with white matter hyperintensities (French et al., 2014). Work is in progress to determine to what extent genetic variation in human *FOXF2* affects the risk to suffer a stroke and to distinguish the relative contributions of *FOXF2* and *FOXC1* to 6p25-stroke associations.

EXPERIMENTAL PROCEDURES

Mouse Strains

For construction of the constitutive (*Foxf2*$^{-}$) and conditional (*Foxf2*^{fl}) *Foxf2* null alleles, see Supplemental Experimental Procedures. To ensure that the observed knockout phenotype was allele independent, key experiments were repeated with a *Foxf2*$^{-}$ allele kindly provided by Dr N. Miura (Wang et al., 2003).

The *Tg*(*FOXF2*) transgenic strain and rescue of the null allele by this transgene has been described elsewhere (Nik et al., 2013). *mTmG* (Muzumdar et al., 2007), *Wnt1-Cre* (Danielian et al., 1998), *Tie2-Cre* (Kisanuki et al., 2001), and *CAGG-Cre*^{ERT2} (Hayashi and McMahon, 2002) strains were obtained from Jackson Laboratories, and the *Foxs1*^{lacZ} knockin (Heglind et al., 2005) was kindly provided by Dr S. Enerbäck.

All mutants were maintained on C57Bl/6 background (Charles River) with some 129/SvJ contribution. Experiments were approved by the Gothenburg Animal Ethics Committee.

Pericyte Quantification and Proliferation Assay

Brains from *Foxs1*$^{lacZ/+}$ embryos, or adults, were fixed in 4% paraformaldehyde (trans-cardiac perfusion for E18.5 and adults), stained with X-gal according to Hogan et al. (1994), and sectioned (paraffin, 6 μm). Brain pericytes were quantified by counting β-gal+ cells in the brain parenchyma in several matching pairs of sections from mutant and wild-type (three or more individuals per genotype). To quantify proliferation, the dam was injected with BrdU (Sigma-Aldrich; 100 μg/g body weight) 1 hr prior to euthanasia, and the percentage

of β-gal+ nuclei in the brain that were also BrdU+ was compared between littermates of different genotype.

BBB Permeability Assays

Evans blue (Sigma-Aldrich, 1% in PBS) was injected intraperitoneally 3 hr (E18.5, in utero) or 6 hr (adults) before euthanasia. After trans-cardiac perfusion with PBS, the brain was homogenized in NN-dimethylformamide, and Evans blue concentration was measured as A_{620}, according to Su et al. (2008). HRP (Sigma Aldrich; 0.5 mg/g body weight) was injected through the tail vein and allowed to circulate for 15 min before euthanasia and perfusion fixation. DAB cytochemistry on brain vibratome sections, followed by TEM, was performed according to Karnovsky (1967).

Immunodetection and In Situ Hybridization

The anti-Foxf2 antibody HPA004763 is an affinity-purified antibody from the Human Protein Atlas Project (Nik et al., 2013; Pontén et al., 2008). For other primary antibodies used for IHC, immunofluorescence, and western blot, together with details on methods and detection systems, see Supplemental Experimental Procedures. In situ hybridization with ^{35}S-labeled RNA probe on sections counterstained with Richardson's methylene blue/azur II was performed according to Angerer and Angerer (1992) and whole-mount in situ hybridization/vibratome sectioning according to Landgren and Carlsson (2004). Tissues were processed for TEM as previously described (Blixt et al., 2007).

qPCR

cDNA was synthesized (Transcriptor First Strand cDNA Synthesis Kit; Roche) from total RNA prepared from E18.5 or adult brain (GenElute Mammalian Total RNA Miniprep Kit; Sigma-Aldrich) and analyzed by SYBR Green qPCR (5x HOT FIREPol EvaGreen qPCR Mix Plus [ROX]; SOLIS) in triplicate. C_t values were normalized against the 36B4 transcript (Akamine et al., 2007). For primer sequences, see Supplemental Experimental Procedures.

Statistics

ANOVA was used to test how parameters depended on *Foxf2* gene dosage and two-tailed Student's t tests for pairwise comparisons of means. Data points were log-transformed (Evans blue) or arcsine-transformed (fractions) when required to obtain normal distribution. Frequencies of pericyte nuclei in TEM sections were tested with χ^2 analysis.

SUPPLEMENTAL INFORMATION

Supplemental Information includes Supplemental Experimental Procedures and six figures and can be found with this article online at http://dx.doi.org/10.1016/j.devcel.2015.05.008.

ACKNOWLEDGMENTS

We thank Drs. S. Enerbäck (University of Gothenburg) and N. Miura (Hamamatsu University) for mouse strains; the staff at the Center for Cellular Imaging, University of Gothenburg, for assistance with confocal microscopy; and Drs. S. Childs (University of Calgary) and O. Lehmann (University of Alberta) for valuable comments on this paper. This work was supported by grants to P.C. from the Swedish Cancer Foundation and the Swedish Medical Research Council.

Received: March 26, 2014
Revised: February 9, 2015
Accepted: May 12, 2015
Published: June 25, 2015

REFERENCES

Akamine, R., Yamamoto, T., Watanabe, M., Yamazaki, N., Kataoka, M., Ishikawa, M., Ooie, T., Baba, Y., and Shinohara, Y. (2007). Usefulness of the 5′ region of the cDNA encoding acidic ribosomal phosphoprotein P0 conserved among rats, mice, and humans as a standard probe for gene expression analysis in different tissues and animal species. J. Biochem. Biophys. Methods *70*, 481–486.

Anderson, K.D., Pan, L., Yang, X.M., Hughes, V.C., Walls, J.R., Dominguez, M.G., Simmons, M.V., Burfeind, P., Xue, Y., Wei, Y., et al. (2011). Angiogenic sprouting into neural tissue requires Gpr124, an orphan G protein-coupled receptor. Proc. Natl. Acad. Sci. U S A *108*, 2807–2812.

Angerer, L.M., and Angerer, R.C. (1992). In situ hybridization to cellular RNA with radiolabelled RNA probes. In In Situ Hybridization: A Practical Approach, D.G. Wilkinson, ed. (Oxford: Oxford University Press), pp. 15–32.

Armulik, A., Genové, G., Mäe, M., Nisancioglu, M.H., Wallgard, E., Niaudet, C., He, L., Norlin, J., Lindblom, P., Strittmatter, K., et al. (2010). Pericytes regulate the blood-brain barrier. Nature *468*, 557–561.

Armulik, A., Genové, G., and Betsholtz, C. (2011). Pericytes: developmental, physiological, and pathological perspectives, problems, and promises. Dev. Cell *21*, 193–215.

Arnold, T.D., Niaudet, C., Pang, M.F., Siegenthaler, J., Gaengel, K., Jung, B., Ferrero, G.M., Mukouyama, Y.S., Fuxe, J., Akhurst, R., et al. (2014). Excessive vascular sprouting underlies cerebral hemorrhage in mice lacking αVβ8-TGFβ signaling in the brain. Development *141*, 4489–4499.

Astorga, J., and Carlsson, P. (2007). Hedgehog induction of murine vasculogenesis is mediated by Foxf1 and Bmp4. Development *134*, 3753–3761.

Bader, B.L., Rayburn, H., Crowley, D., and Hynes, R.O. (1998). Extensive vasculogenesis, angiogenesis, and organogenesis precede lethality in mice lacking all alpha v integrins. Cell *95*, 507–519.

Blixt, A., Landgren, H., Johansson, B.R., and Carlsson, P. (2007). Foxe3 is required for morphogenesis and differentiation of the anterior segment of the eye and is sensitive to Pax6 gene dosage. Dev. Biol. *302*, 218–229.

Cambier, S., Gline, S., Mu, D., Collins, R., Araya, J., Dolganov, G., Einheber, S., Boudreau, N., and Nishimura, S.L. (2005). Integrin alpha(v)beta8-mediated activation of transforming growth factor-beta by perivascular astrocytes: an angiogenic control switch. Am. J. Pathol. *166*, 1883–1894.

Cellini, E., Disciglio, V., Novara, F., Barkovich, J.A., Mencarelli, M.A., Hayek, J., Renieri, A., Zuffardi, O., and Guerrini, R. (2012). Periventricular heterotopia with white matter abnormalities associated with 6p25 deletion. Am. J. Med. Genet. A. *158A*, 1793–1797.

Daneman, R., Zhou, L., Kebede, A.A., and Barres, B.A. (2010). Pericytes are required for blood-brain barrier integrity during embryogenesis. Nature *468*, 562–566.

Danielian, P.S., Muccino, D., Rowitch, D.H., Michael, S.K., and McMahon, A.P. (1998). Modification of gene activity in mouse embryos in utero by a tamoxifen-inducible form of Cre recombinase. Curr. Biol. *8*, 1323–1326.

Etchevers, H.C., Vincent, C., Le Douarin, N.M., and Couly, G.F. (2001). The cephalic neural crest provides pericytes and smooth muscle cells to all blood vessels of the face and forebrain. Development *128*, 1059–1068.

Foster, K., Sheridan, J., Veiga-Fernandes, H., Roderick, K., Pachnis, V., Adams, R., Blackburn, C., Kioussis, D., and Coles, M. (2008). Contribution of neural crest-derived cells in the embryonic and adult thymus. J. Immunol. *180*, 3183–3189.

French, C.R., Seshadri, S., Destefano, A.L., Fornage, M., Arnold, C.R., Gage, P.J., Skarie, J.M., Dobyns, W.B., Millen, K.J., Liu, T., et al. (2014). Mutation of FOXC1 and PITX2 induces cerebral small-vessel disease. J. Clin. Invest. *124*, 4877–4881.

Gaengel, K., Genové, G., Armulik, A., and Betsholtz, C. (2009). Endothelial-mural cell signaling in vascular development and angiogenesis. Arterioscler. Thromb. Vasc. Biol. *29*, 630–638.

Goumans, M.-J., Valdimarsdottir, G., Itoh, S., Rosendahl, A., Sideras, P., and ten Dijke, P. (2002). Balancing the activation state of the endothelium via two distinct TGF-beta type I receptors. EMBO J. *21*, 1743–1753.

Goumans, M.J., Valdimarsdottir, G., Itoh, S., Lebrin, F., Larsson, J., Mummery, C., Karlsson, S., and ten Dijke, P. (2003). Activin receptor-like kinase (ALK)1 is an antagonistic mediator of lateral TGFbeta/ALK5 signaling. Mol. Cell *12*, 817–828.

Hawkins, B.T., and Egleton, R.D. (2006). Fluorescence imaging of blood-brain barrier disruption. J. Neurosci. Methods *151*, 262–267.

Hayashi, S., and McMahon, A.P. (2002). Efficient recombination in diverse tissues by a tamoxifen-inducible form of Cre: a tool for temporally regulated gene activation/inactivation in the mouse. Dev. Biol. *244*, 305–318.

Heglind, M., Cederberg, A., Aquino, J., Lucas, G., Ernfors, P., and Enerbäck, S. (2005). Lack of the central nervous system- and neural crest-expressed forkhead gene Foxs1 affects motor function and body weight. Mol. Cell. Biol. *25*, 5616–5625.

Hellström, M., Kalén, M., Lindahl, P., Abramsson, A., and Betsholtz, C. (1999). Role of PDGF-B and PDGFR-beta in recruitment of vascular smooth muscle cells and pericytes during embryonic blood vessel formation in the mouse. Development *126*, 3047–3055.

Hirschi, K.K., Burt, J.M., Hirschi, K.D., and Dai, C. (2003). Gap junction communication mediates transforming growth factor-beta activation and endothelial-induced mural cell differentiation. Circ. Res. *93*, 429–437.

Hogan, B., Beddington, R., Costantini, F., and Lacy, E. (1994). Manipulating the Mouse Embryo: A Laboratory Manual, Second Edition (New York: Cold Spring Harbor Laboratory Press).

Iwata, J., Hacia, J.G., Suzuki, A., Sanchez-Lara, P.A., Urata, M., and Chai, Y. (2012). Modulation of noncanonical TGF-β signaling prevents cleft palate in Tgfbr2 mutant mice. J. Clin. Invest. *122*, 873–885.

Jakobsen, J.S., Braun, M., Astorga, J., Gustafson, E.H., Sandmann, T., Karzynski, M., Carlsson, P., and Furlong, E.E.M. (2007). Temporal ChIP-on-chip reveals Biniou as a universal regulator of the visceral muscle transcriptional network. Genes Dev. *21*, 2448–2460.

Kapoor, S., Mukherjee, S.B., Shroff, D., and Arora, R. (2011). Dysmyelination of the cerebral white matter with microdeletion at 6p25. Indian Pediatr. *48*, 727–729.

Karnovsky, M.J. (1967). The ultrastructural basis of capillary permeability studied with peroxidase as a tracer. J. Cell Biol. *35*, 213–236.

Kisanuki, Y.Y., Hammer, R.E., Miyazaki, J., Williams, S.C., Richardson, J.A., and Yanagisawa, M. (2001). Tie2-Cre transgenic mice: a new model for endothelial cell-lineage analysis in vivo. Dev. Biol. *230*, 230–242.

Korn, J., Christ, B., and Kurz, H. (2002). Neuroectodermal origin of brain pericytes and vascular smooth muscle cells. J. Comp. Neurol. *442*, 78–88.

Kurz, H. (2009). Cell lineages and early patterns of embryonic CNS vascularization. Cell Adh. Migr. *3*, 205–210.

Landgren, H., and Carlsson, P. (2004). FoxJ3, a novel mammalian forkhead gene expressed in neuroectoderm, neural crest, and myotome. Dev. Dyn. *231*, 396–401.

Levéen, P., Pekny, M., Gebre-Medhin, S., Swolin, B., Larsson, E., and Betsholtz, C. (1994). Mice deficient for PDGF B show renal, cardiovascular, and hematological abnormalities. Genes Dev. *8*, 1875–1887.

Li, F., Lan, Y., Wang, Y., Wang, J., Yang, G., Meng, F., Han, H., Meng, A., Wang, Y., and Yang, X. (2011). Endothelial Smad4 maintains cerebrovascular integrity by activating N-cadherin through cooperation with Notch. Dev. Cell *20*, 291–302.

Lindahl, P., Johansson, B.R., Levéen, P., and Betsholtz, C. (1997). Pericyte loss and microaneurysm formation in PDGF-B-deficient mice. Science *277*, 242–245.

Mahlapuu, M., Enerbäck, S., and Carlsson, P. (2001a). Haploinsufficiency of the forkhead gene Foxf1, a target for sonic hedgehog signaling, causes lung and foregut malformations. Development *128*, 2397–2406.

Mahlapuu, M., Ormestad, M., Enerbäck, S., and Carlsson, P. (2001b). The forkhead transcription factor Foxf1 is required for differentiation of extra-embryonic and lateral plate mesoderm. Development *128*, 155–166.

Muzumdar, M.D., Tasic, B., Miyamichi, K., Li, L., and Luo, L. (2007). A global double-fluorescent Cre reporter mouse. Genesis *45*, 593–605.

Nik, A.M., Reyahi, A., Pontén, F., and Carlsson, P. (2013). Foxf2 in intestinal fibroblasts reduces numbers of Lgr5(+) stem cells and adenoma formation by inhibiting Wnt signaling. Gastroenterology *144*, 1001–1011.

Ormestad, M., Astorga, J., and Carlsson, P. (2004). Differences in the embryonic expression patterns of mouse Foxf1 and -2 match their distinct mutant phenotypes. Dev. Dyn. *229*, 328–333.

Ormestad, M., Astorga, J., Landgren, H., Wang, T., Johansson, B.R., Miura, N., and Carlsson, P. (2006). Foxf1 and Foxf2 control murine gut development by limiting mesenchymal Wnt signaling and promoting extracellular matrix production. Development *133*, 833–843.

Pontén, F., Jirström, K., and Uhlen, M. (2008). The Human Protein Atlas—a tool for pathology. J. Pathol. *216*, 387–393.

Rosenberg, R.E., Egan, M., Rodgers, S., Harter, D., Burnside, R.D., Milla, S., and Pappas, J. (2013). Complex chromosome rearrangement of 6p25.3- > p23 and 12q24.32- > qter in a child with moyamoya. Pediatrics *131*, e1996–e2001.

Sato, Y., and Rifkin, D.B. (1989). Inhibition of endothelial cell movement by pericytes and smooth muscle cells: activation of a latent transforming growth factor-beta 1-like molecule by plasmin during co-culture. J. Cell Biol. *109*, 309–315.

Shi, M., Zhu, J., Wang, R., Chen, X., Mi, L., Walz, T., and Springer, T.A. (2011). Latent TGF-β structure and activation. Nature *474*, 343–349.

Siegenthaler, J.A., Choe, Y., Patterson, K.P., Hsieh, I., Li, D., Jaminet, S.C., Daneman, R., Kume, T., Huang, E.J., and Pleasure, S.J. (2013). Foxc1 is required by pericytes during fetal brain angiogenesis. Biol. Open *2*, 647–659.

Soriano, P. (1994). Abnormal kidney development and hematological disorders in PDGF beta-receptor mutant mice. Genes Dev. *8*, 1888–1896.

Su, E.J., Fredriksson, L., Geyer, M., Folestad, E., Cale, J., Andrae, J., Gao, Y., Pietras, K., Mann, K., Yepes, M., et al. (2008). Activation of PDGF-CC by tissue plasminogen activator impairs blood-brain barrier integrity during ischemic stroke. Nat. Med. *14*, 731–737.

van der Knaap, M.S., Kriek, M., Overweg-Plandsoen, W.C., Hansson, K.B., Madan, K., Starreveld, J.S., Schotman-Schram, P., Barkhof, F., and Lesnik Oberstein, S.A. (2006). Cerebral white matter abnormalities in 6p25 deletion syndrome. AJNR Am. J. Neuroradiol. *27*, 586–588.

Vernon, H.J., Bytyci Telegrafi, A., Batista, D., Owegi, M., and Leigh, R. (2013). 6p25 microdeletion: white matter abnormalities in an adult patient. Am. J. Med. Genet. A. *161A*, 1686–1689.

Wang, T., Tamakoshi, T., Uezato, T., Shu, F., Kanzaki-Kato, N., Fu, Y., Koseki, H., Yoshida, N., Sugiyama, T., and Miura, N. (2003). Forkhead transcription factor Foxf2 (LUN)-deficient mice exhibit abnormal development of secondary palate. Dev. Biol. *259*, 83–94.

Winkler, E.A., Bell, R.D., and Zlokovic, B.V. (2011). Central nervous system pericytes in health and disease. Nat. Neurosci. *14*, 1398–1405.

Wipff, P.-J., and Hinz, B. (2008). Integrins and the activation of latent transforming growth factor β1 - an intimate relationship. Eur. J. Cell Biol. *87*, 601–615.

Yamanishi, E., Takahashi, M., Saga, Y., and Osumi, N. (2012). Penetration and differentiation of cephalic neural crest-derived cells in the developing mouse telencephalon. Dev. Growth Differ. *54*, 785–800.

Zhu, J., Motejlek, K., Wang, D., Zang, K., Schmidt, A., and Reichardt, L.F. (2002). beta8 integrins are required for vascular morphogenesis in mouse embryos. Development *129*, 2891–2903.

Zlokovic, B.V. (2008). The blood-brain barrier in health and chronic neurodegenerative disorders. Neuron *57*, 178–201.